CAAP Quarterly Report
March 30th, 2025

Project Name: Development of a Framework for Assessing Cathodic Protection (CP) Effectiveness in Pipelines Based on Artificial Intelligence (AI)

Contract Number: 693JK32350005CAAP

Prime University: ***Texas A&M Engineering Experiment Station***

Prepared By: PI Homero Castaneda-Lopez Professor, hcastaneda@tamu.edu,
phone: 9794589844

Reporting Period: January 1st – March 31st, 2025

Project Activities for Reporting Period:

Task 1. Designing and building the physical prototypes in laboratory conditions and deterministic modeling.

In continued efforts to create a deterministic model for modeling the potential distribution in cathodically protected pipelines, validation was performed both on the lab and field scale. Validation on the lab scale was continued by comparing the output of the 2D TLM using mechanistic definitions for the interface impedance with experimental data. To begin validating the model in the larger field scale, the initial model was extended to a quasi-1D case where the x-direction of the model (length of the pipeline) is on the order of kilometers while the y-direction (circumference of the pipeline) is on the order of meters.

To first verify the validity of the numerical model, it was compared with a commonly used analytical model that explains the potential distribution in a buried pipeline under cathodic protection. For a homogenous system with constant soil resistance and coating impedance, the analytical solution for the potential distribution was defined as:

$$\Phi(x) = \Phi_{min}\cosh(\alpha(l-x)) \quad (1)$$

$$\Phi_{applied} = \Phi_{min}\cosh(\alpha l) \quad (2)$$

$$\alpha = \sqrt{\frac{Rs}{Z}} \quad (3)$$

The boundary conditions for the system are at $x = 0,\ \Phi = \Phi_{applied}$ and $x = l,\ \Phi = \Phi_{min}$, where Φ_{min} was assumed to be $-850\ mV\ vs\ CSE$ and $\Phi_{applied}$ was the minimum potential needed to be applied to reach the minimum potential at the end of the pipeline. Figure 1 shows the comparison of the TLM with both homogenous and heterogenous coating conditions with the analytical solution.

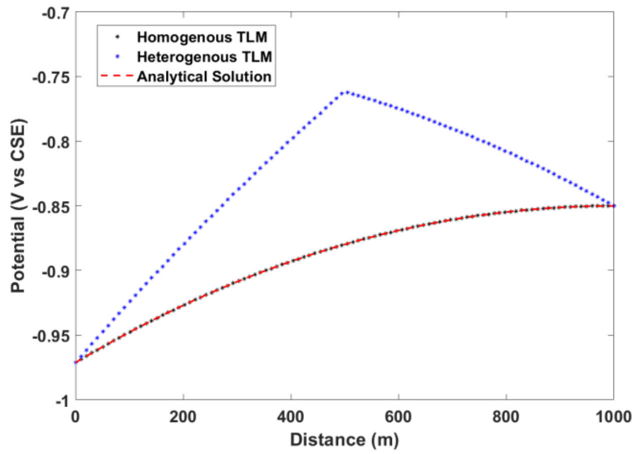

Figure 1: Comparison of TLM output with analytical solution. Parameters used in the model are: $\boldsymbol{\sigma_s = 150\frac{\mu S}{cm}, R_{coating} = 1e6\frac{\Omega}{m},\ R_{holiday} = 5.75e2\frac{\Omega}{m}, \Phi_{min} = -0.850\ VvsCSE, \Phi_{applied} = -0.971\ VvsECSE}$

From Figure 1 it can be seen that the homogenous TLM output agrees with the analytical solution with little to no deviation between the two outputs. With the introduction of a low impedance segment to the pipeline there was a fundamental change in the potential distribution compared to the homogenous case. Showing that with the proper definition of impedance terms and distribution of impedance and soil resistivity values it is possible to simulate potential maps for buried pipeline systems.

Numerical analysis of the potential distribution model was performed to understand the effects of input parameters on the resulting potential profiles. Analysis was performed for finite pipelines and infinite pipelines, the key difference between the two assumptions are the boundary conditions at left and right boundaries of the model. For finite pipelines it is assumed that at the boundaries the assumed potential is at the minimum protection potential, while for infinite case the potential approaches zero as the distance goes towards infinity. Figure 2 and

Figure 3 show the effect of soil resistivity and coating impedance on the potential distribution for pipelines with singular or multiple potential application points. With changing soil resistivity, it can be seen that with increasing resistivity there is a faster change in potential towards more positive values relative to lower resistivities. This can be clearly seen in Figure 2b where with a change from 1e4 to 1e5 Ω-cm the potential at the boundary goes from around -1.25 V vs CSE to near -0.850 V vs CSE. With the application of potential at multiple sites across the pipeline it is possible to stay below -0.850 V vs CSE even in the higher resistive media. For a system with only a single potential application point and soil resistivity of 1e6 Ω-cm potential quickly rises to around -0.850 V vs SCE, but will multiple potential application sites the modeled potential stays below -1V vs CSE over the entire domain.

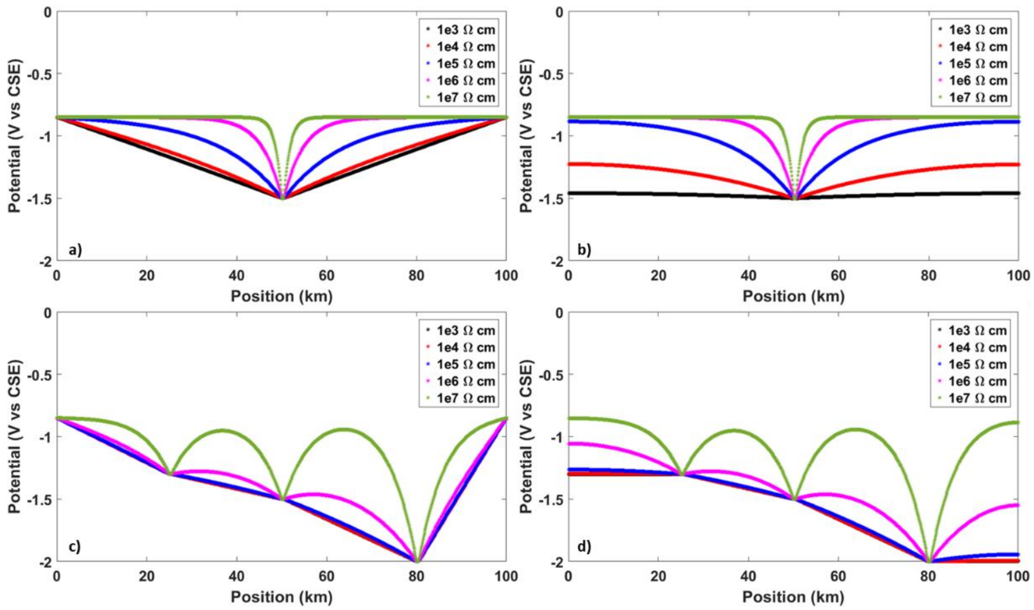

Figure 2: Effect of soil resistivity on a) finite and b) infinite pipeline with single potential application point, and c) finite and d) infinite pipeline with multiple potential application points.

The overall effect of coating impedance on the potential distribution occurred over a much smaller region compared to the role of soil resistivity. With changing coating impedance, it can be seen that with decreasing coating impedance, there is a faster change in potential towards more positive values relative to higher coating impedances. In

Figure **3**b it can be seen that with just a single order of magnitude difference, there is a large change in the potential distribution behavior between the two pipelines. Using multiple potential application points was not as to keep the modeled potential distribution below the minimum potential level. The overall potential distribution is sensitive to both soil resistivity and coating impedance values, but the system is more sensitive to smaller changes in coating impedance compared to the soil resistivity.

Figure 4a shows the effect of heterogeneous soil resistivity and coating impedance on the potential distribution for a pipeline with multiple potential application sites. The spatial distribution of the soil resistivity and coating impedance is shown in Figure 4b and c, respectively. It was assumed that the coating impedance was varied discretely between 3.81e13, 1.91e13, 1.91e12, and 7.62e11 Ω-cm^2 at the measurement points along the pipeline.

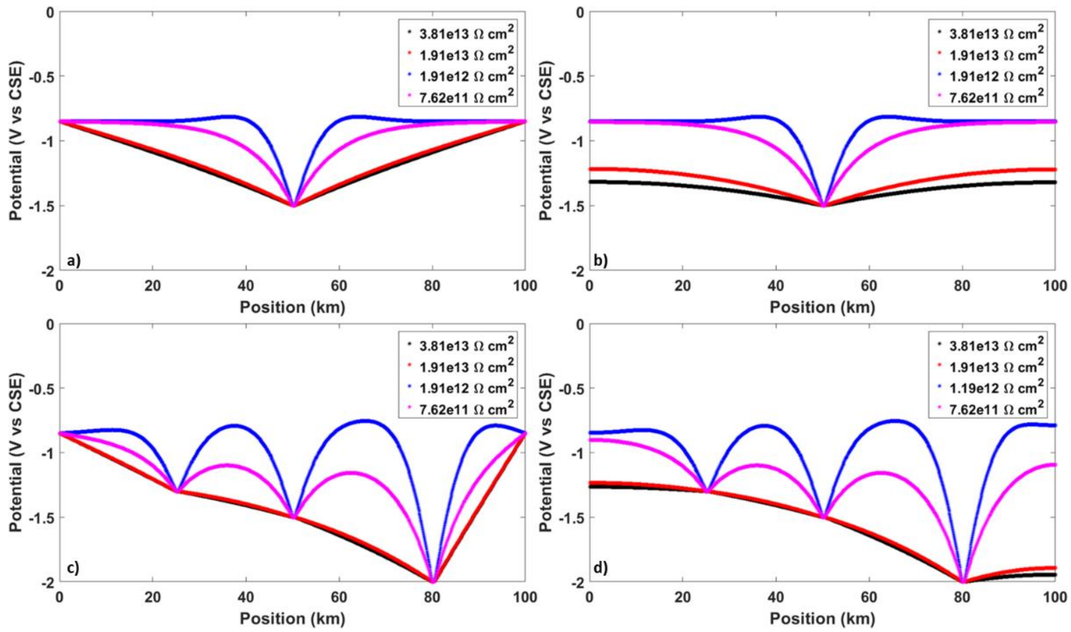

Figure 3: Effect of soil resistivity on a) finite and b) infinite pipeline with single potential application point, and c) finite and d) infinite pipeline with multiple potential application points.

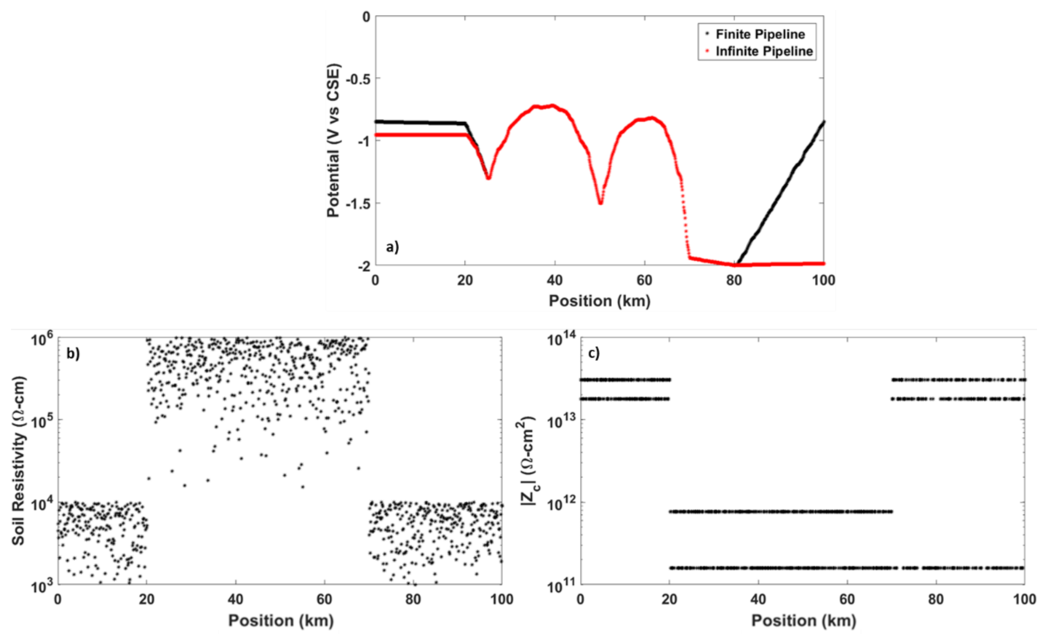

Figure 4: a) Effect of heterogeneous soil resistance and coating impedance on pipeline with multiple potential application points, b) Soil resistivity distribution, and c) coating impedance distribution.

From 0 to 20 km, it was assumed that the coating impedance could be either of the two highest impedance values at each measurement point, and from 20 to 70 km, it was assumed it could be either of the two lowest impedance values. For the last segment of the pipeline, it was assumed that the coating impedance could vary between the two highest and lowest impedance values at each measurement point. This was done to see the effect of large local changes (roughly one order of magnitude) on the potential distribution of the pipeline. In the first region from 0 to 20 km the average coating impedance was the highest for the modeled pipeline and coupling, and with a relatively low soil resistivity, there was little to no potential drop occurring in this region. From 20 to 70 km, there is a region of higher soil resistivity coupled with relatively low coating impedance displaying high rates of potential change over the region. For both of the potential application points, there is //a sharp increase in the modeled potential. In both regions where there was a higher average coating impedance, the overall potential change was less steep.

Task 2: Integrating field inspection, theoretical, with experimental data by applying pattern recognition techniques relating the pipeline-coating-soil system with CP.

For initial validation of the TLM potential distribution, it was compared with the ON potential measurements for field CIPS measurements on a 56 km buried pipeline with two rectifier locations. For the best fit between the model and field data, there were four different ways of estimating the coating impedance over the length of the pipeline:

1. Constant coating impedance value for the entire pipeline
2. Discrete distribution of coating impedance at each measurement location
3. Normal distribution of coating impedance with a single mean value for the entire pipeline
4. Normal distribution of coating impedance with multiple mean values for the entire pipeline

For simulating the field data, the soil resistivity used in the model was the measured soil resistivity values collected along the length of the pipeline. Figure 5a shows the measured soil resistivity data in Ω-km, and Figures b and c compare the model output (red line) with field data (black dots) using the first two methods of assuming the coating impedance distribution. Using a homogenous value of the coating impedance was able to generally follow the trend of the potential distribution but was underestimating the potential values compared to the field data. In Figure 5c the two discrete values used for the coating impedance were $R_{C1} = 2.76\ \Omega\ km^2$ $R_{C2} = 0.276\ \Omega\ km^2$, At each measurement point in the model the impedance value was randomly chosen to be either one of these two values. This allowed a better fitting compared to the homogenous case, but had still had some large deviations between the model output and field data.

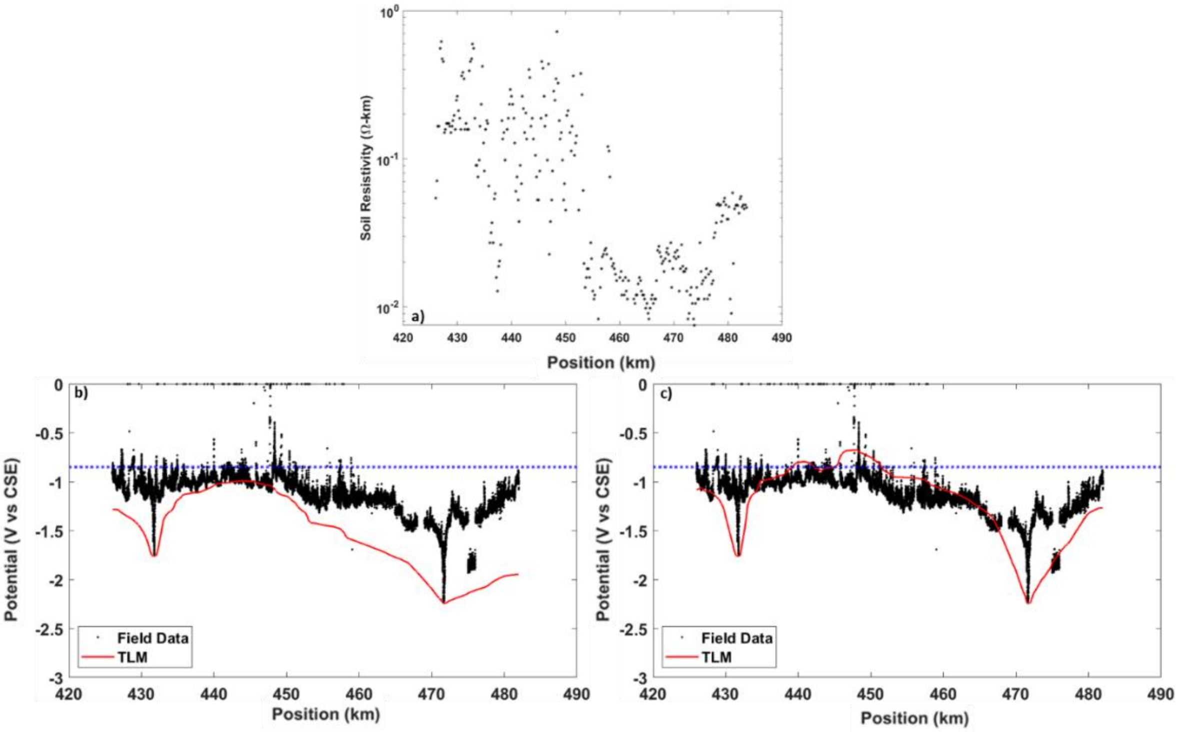

Figure 5: a) Soil Resistivity distribution, Comparison of TLM potential distribution with field CIPS data for b) homogenous coating impedance ($\boldsymbol{R_C = 2.76\ \Omega\ km^2}$), and c) heterogenous coating with discrete coating impedance distribution ($\boldsymbol{R_{C1} = 2.76\ \Omega\ km^2\ \ R_{C2} = 0.276\ \Omega\ km^2}$)

Figure 6a and c compare the model output with field data for various coating impedance assumption cases 3 and 4, respectively. The assumed coating impedance distribution for both cases is shown in Figuresb and d. The assumed coating impedance model input parameters are shown in

Table 1. From Figure 6a it can be seen that using a normally distributed impedance parameter was able to provide a relatively good fit between model and field data around the 5 to 25 km section of the pipeline. In the other regions, the assumed coating impedance was not able to accurately describe the assumed potential distribution. In Figure 6c, the model output was relatively close to the measured values, providing a good estimation of the coating impedance along the length of the pipeline.

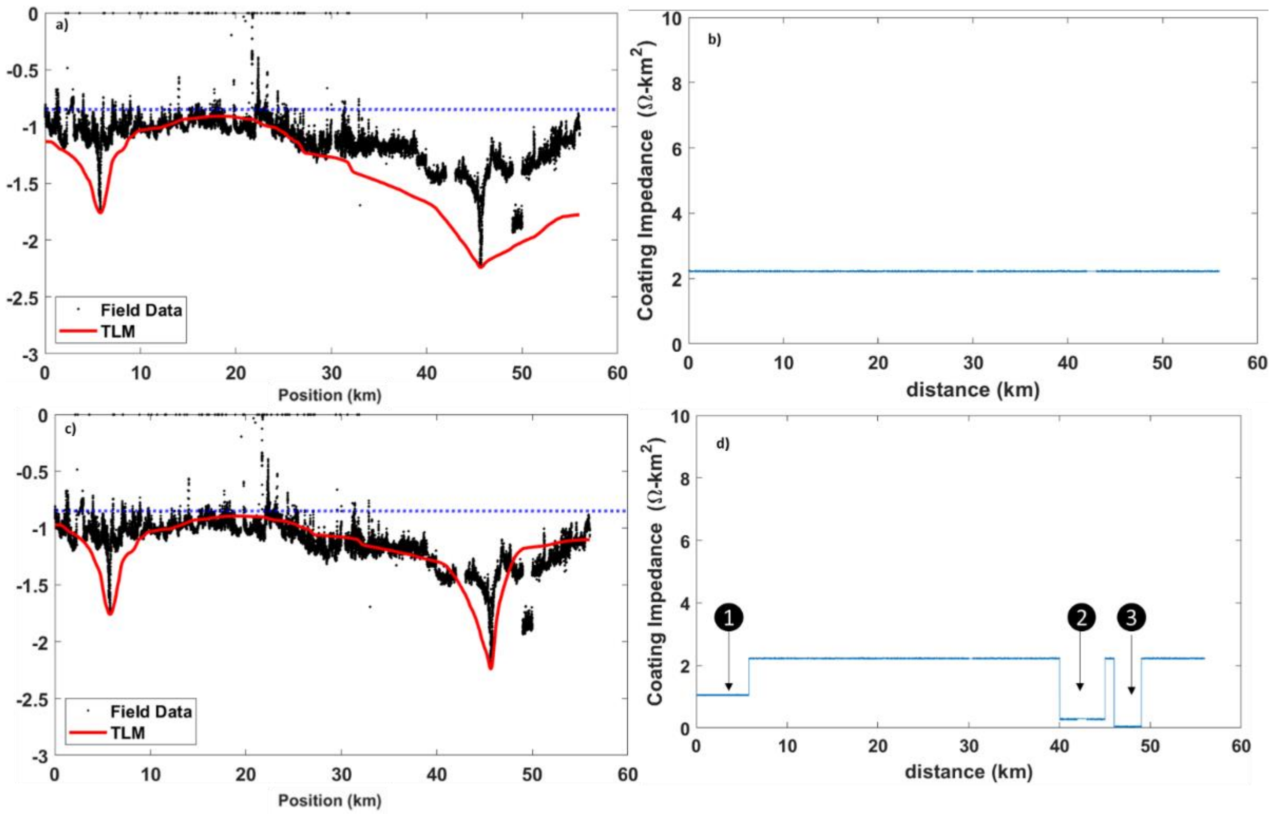

Figure 6: a,c) Comparison of model potential distribution with field CIPS using a single impedance mean value and a distribution of mean impedance values, and b,d) coating impedance distribution along the length of the pipeline

Table 1: Model parameters for calculating potential distribution

	x_i (km)	x_f (km)	μ_{Rc} (Ω-km^2)	σ_{Rc} (Ω-km^2)
Baseline	---	---	2.225	0.01
Segment 1	0	5.77	1.047	0.01
Segment 2	40	45	0.2762	0.01
Segment 3	46	49	0.0381	0.01

References

1. Q. Zhao, V. Hautamaki and P. Fränt, "20 Q. Zhao, V. Hautamaki and P. Fränti, "Knee Point Detection in BIC for Detecting the Number of Clusters", ACIVS, 2008," in

International conference on advanced concepts for intelligent vision systems*, Berlin, 2008.
2. A. Kowalski, "The close interval potential survey (CIS/CIPS) method for detecting corrosion in underground pipelines," in *Underground pipeline corrosion*, Elsevier, 2014, pp. 227-246.

Task 3: Validation of the *a priori* framework with experimental and field conditions for characterization/modeling and Evaluation/Validation

Physics-Based Bayesian Optimization for Severity Estimation Using CIPS Readings in Underground Pipelines

Ensuring the structural integrity of underground pipelines is critical for preventing failures and optimizing maintenance strategies. Close Interval Potential Survey (CIPS) is widely used to assess the effectiveness of cathodic protection systems and detect potential corrosion-related defects. However, conventional methods for interpreting CIPS data often rely on empirical thresholds or deterministic models, which may not adequately capture uncertainties in defect severity estimation. Hence based on the Transmission Line Model (TLM) model developed by Texas A&M university we propose a Physics-Based Bayesian Optimization (PBBO) model that integrates the Transmission Line Model (TLM) to simulate potential distribution along underground pipelines, capturing the electrochemical and physical effects influencing CIPS readings. By incorporating Bayesian optimization, the model systematically refines severity estimation by learning from prior corrosion data, accounting for uncertainties, and improving defect localization.

In the proposed model, known inputs include soil resistivity along the pipeline ($\boldsymbol{R_s}$), coating resistance ($\boldsymbol{R_c}$), CIPS voltage readings along the pipeline ($\boldsymbol{V_m}$), locations of cathodic protection (CP) rectifiers($\boldsymbol{X_m}$), and possible defect (holiday) locations ($\boldsymbol{X_h}$) identified from CIPS readings. The primary objective is to estimate the holiday resistance ($\boldsymbol{R_h}$) and capacitance ($\boldsymbol{C_h}$) at the defect locations, as these parameters directly indicate the severity of pipeline degradation.
The random variables in this model are: $\boldsymbol{R_h}$, $\boldsymbol{C_h}$ and rectifier voltages $\boldsymbol{V_r} = [V_1, V_2, V_3 \dots . V_l\,]$ for l rectifiers. Given that there are k holidays and l rectifiers, the model includes a total of $2k + l + 1$ random variables. We define prior distributions for $\boldsymbol{R_h}$ and $\boldsymbol{C_h}$ as normal distributions based on the properties of bare ($R_{s,}\, C_{s)}$

$$\boldsymbol{R_h} \sim N(R_s, \Sigma_s)\,, \qquad \boldsymbol{C_h} \sim N(C_s, \Sigma_s).$$

The rectifier voltages $\boldsymbol{V_r}$ are also assumed to be normally distributed, with values expected to fall within the NACE-recommended protection range of -0.85V to -1.2V, beyond which the pipeline is considered overprotected. Thus, the model parameters are represented as:

$$\boldsymbol{\Theta} = [\boldsymbol{R_h}, \boldsymbol{C_h}, \boldsymbol{V_r}].$$

Figure 7 shows the probabilistic graph model (PGM) for the proposed Bayesian model. A PGM is a visual and mathematical representation of the probabilistic relationships between random variables using nodes and edges. It helps capture dependencies, encode joint distributions efficiently, and is widely used in Bayesian inference, machine learning, and uncertainty quantification. Given sampled values of the parameter vector $\boldsymbol{\Theta}$, the predicted CP potential (V_p) is computed using the TLM forward model. In practice, the predicted values ($\boldsymbol{V_p}$) rarely match the measured CIPS values ($\boldsymbol{V_m}$) perfectly due to model inaccuracies, environmental uncertainties, and data noise. This discrepancy is represented by an error term $\boldsymbol{\varepsilon}$, which is assumed to be independently and identically distributed as:

$$\boldsymbol{\varepsilon} = N(0, \boldsymbol{\sigma_\varepsilon^2}).$$

According to Bayesian literature [1][2] a noninformative prior (weakly informative prior) like an inverse gamma distribution ($\boldsymbol{\Gamma^{-1}}(\boldsymbol{\alpha_{\sigma_\varepsilon}}, \boldsymbol{\beta_{\sigma_\varepsilon}})$) can be assumed as prior for the variance ($\boldsymbol{\sigma_\varepsilon^2}$) of the model. Thus, the components of the Bayesian model are defined as,

$$Prior\big((\boldsymbol{p} = (\boldsymbol{\Theta}, \boldsymbol{\sigma_\varepsilon})\big) = \prod_i^N N(\boldsymbol{\Theta_i}, \boldsymbol{\mu_{\Theta_i}}, \boldsymbol{\Sigma_{\Theta_i}}) \times \boldsymbol{\Gamma^{-1}}(\boldsymbol{\sigma_\varepsilon}; \boldsymbol{\alpha_{\sigma_\varepsilon}}, \boldsymbol{\beta_{\sigma_\varepsilon}})$$

$$Likelihood(\boldsymbol{\varepsilon}|\boldsymbol{p}) = \prod_i^N N(\boldsymbol{\varepsilon}; \boldsymbol{0}, \boldsymbol{\sigma_\varepsilon^2})$$

Given the prior and likelihood, the posterior according to Bayes theorem is,

$$post(\boldsymbol{p}|\boldsymbol{\varepsilon}) \propto \boldsymbol{\Gamma^{-1}}(\boldsymbol{\sigma_\varepsilon}; \boldsymbol{\alpha_{\sigma_\varepsilon}}, \boldsymbol{\beta_{\sigma_\varepsilon}}) \times \prod_i^N N(\boldsymbol{\Theta}; \boldsymbol{\mu_\Theta}, \boldsymbol{\Sigma_\Theta}) N(\boldsymbol{\varepsilon}; \boldsymbol{0}, \boldsymbol{\sigma_\varepsilon^2})$$

where N is the number of observed data.

Bayesian updating is performed using the No-U-Turn Sampler (NUTS) [3], a variant of Hamiltonian Monte Carlo, which efficiently explores the high-dimensional parameter space and samples from the joint posterior distribution. The resulting samples form a trace of the Markov chain, providing a numerical approximation to the posterior and enabling uncertainty-aware predictions. This probabilistic framework allows for more accurate and interpretable severity estimation, ultimately supporting better decision-making for pipeline integrity management and maintenance planning.

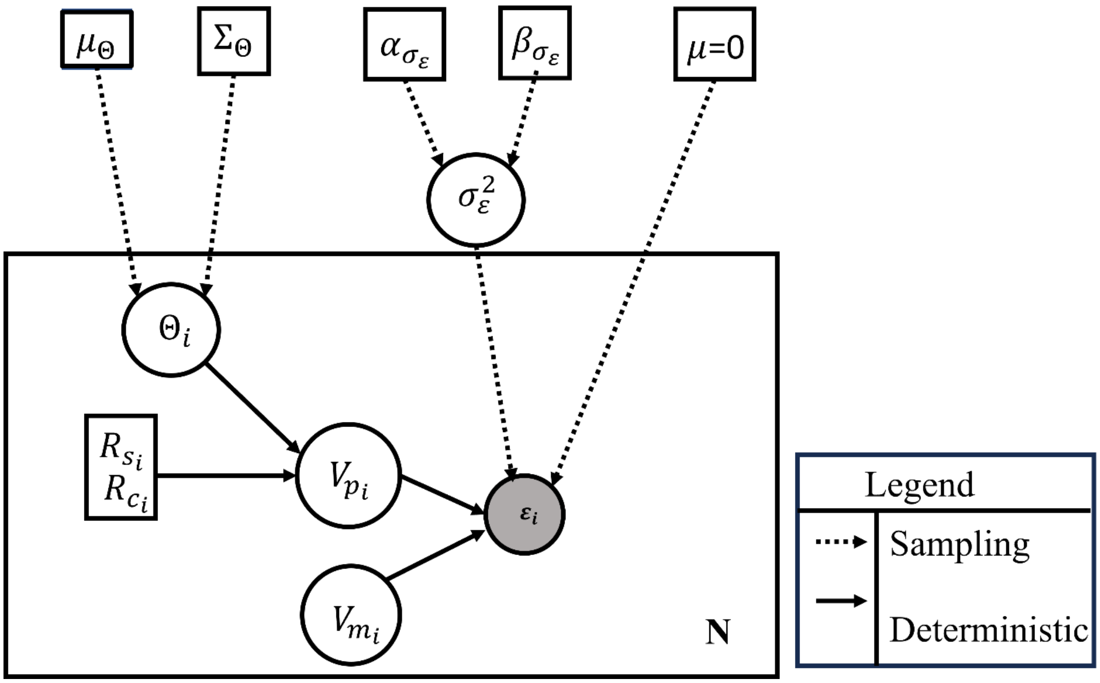

Figure 7: Probabilistic graph model

References:

1. Gelman, J. B. Carlin, H. S. Stern, D. B. Dunson, A. Vehtari and D. B. Rubin, Bayesian Data Analysis(3rd ed.), Chapman and Hall/CRC, 2013.
2. C. M. Bishop, Pattern Recognition and Machine Learning, Cambridge: Springer, 2006.
3. M. D. Hoffman and A. Gelman, "The No-U-Turn sampler: adaptively setting path lengths in Hamiltonian Monte Carlo," *Journal of Machine Learning Research,* vol. 15, no. 1, pp. 1593--1623, 2014.

Project Financial Activities Incurred during the Reporting Period:

- Two PhD students have been involved in the project since January 2025. One full-time employee will perform task 1 and analyze and process data for task 2. One part-time PhD and Master's student will help perform the testing methods to extend the TLM with the AI integration for task No. 3. We added a new undergraduate student for testing and data analysis activities for task 1.
- The UDayton team includes Sreelakshmi Sreeharan as a Postdoc researcher and one PhD student in this project, and continues efforts in Tasks 2 and 3.
- We will attend the AMPP 2025 conference to be held in Nashville, Tennessee. April 2025, and we are preparing two peer review papers for the Journal of Science and Engineering of Pipelines by Elsevier. We are filling a copyright for the TLM for CP and holiday detection.
- The laboratory has been used for several setups and measurements. The simulation of buried conditions has been performed during this and the next quarter. We will use different

high-resolution characterization tools during the laboratory work, such as local electrochemical impedance spectroscopy.

Financial Summary

- Federal Cost Activities (cumulative):
  - PI/Co-PIs/students' involvement and tuition (including total):
    Total: $92,009.68 USD
  - Materials purchased/travel/contractual (consultants/subcontractors):

    Total is: USD 71,728.83

    Total Direct costs: USD 163,738.51

    Total Indirect costs: $38,444.56 USD

    Total: $202,183.07 USD

- Cost Share Activities:
  - Cost share contribution:

- Heuristech has contributed $23,400 in technology training and/or company personnel hours for physical laboratory testing and mathematical tools.
- Integrity Solutions has made the database available with a very high value; the contribution is beyond USD 86,000 ***in CP field data (CIPS, DCVG, Resistivity, historical data, and different rights of ways) base collection***. Also, IS has contributed as a co-share in technical staff resources to collect, collate, evaluate, screen, database development, attending workshops and training, analyzing Cathodic Protection (CP) data, contributing to computer algorithm development programming, and other program software/model components.
- The University of Dayton has contributed $45,939.60 in cost share, $30,524.46 in faculty payroll and $15,415.104 in indirect costs.

Project Activities with Cost Share Partners:

During the sixth quarter of this project, we met several times (around five) with the co-sharing partners; the following outcomes from the meeting were:

- Meetings for updates on the experimental testing for reflectometry methodology.
- Integral Solutions facilitates the collection of databases needed in this project. We have a meeting to clarify the data set and the formatting.
- We will organize a technical workshop with the team partners to get feedback on our proposal concept. We will include some students to train them in the pipeline subject.

Project Activities with External Partners:

- We will organize a technical workshop with the team partners to get feedback on our proposal concept.
- We will organize different courses for pipeline companies, one of the topics will be integrity and risk.

Potential Project Risks:

We received the US pipeline database and already had the international one. The pipelines to be used for the analysis and this project have been selected. Currently, there are no potential risks.

Future Project Work:

We anticipate following the proposed timeline with no current changes during the next months. We will follow the Gantt chart to mark the progress and plans.
During the next 30, 60, and 90 days, we will perform task 1 activities. We will extend more activities in Task 1. Also, we will continue with Task 2's activities and start with Task 3 for the next 30, 60, and 90 days.
Theoretical work, laboratory work, and current database analysis will be considered for the next quarter.

- Include ways of estimating coating defects activity and severity in the coating impedance model
- Continue validating the model with multiple sets of field data

The timeline and schedule for the project are in the Gantt chart.

Task/Subtask	Fiscal Year											
	2023	2024				2025			2025	2026	2026	2026
	Q4	Q1	Q2	Q3	Q4	Q1	Q2	Q3	Q4	Q1	Q2	Q3
Task 1: Designing and building the physical prototypes in laboratory conditions and deterministic modeling												
Task 2: Integrating field inspection, theoretical, with experimental data by applying pattern recognition techniques relating the pipeline-coating-soil system with CP												
Task 3: Validation of the *a priori* framework with experimental and field conditions for characterization/modeling and Evaluation/Validation												
Task 4: Development and validation of the methodology for ECDA based on CP levels												

Deliverable Milestones are indicated in black*, and in dark green is the extended activities.

Potential Impacts to Pipeline Safety:

During the Transmission Line Modeling, we integrate the algorithms used for Artificial Intelligence. The TLM will add the fundamental approach, as well as the field and laboratory validation. The TLM was developed for multiscale conditions, the macro scale is validated with the field data (from Task 2). The micro conditions have been validated with laboratory-scale experiments (from Tasks 1 and 2)
The potential impact is the results generated for the AI algorithm, the TLM is based on a deterministic and fundamental approach. This can not only show different trends for a buried structure under cathodic protection but also include several features in the RoW, resistivity, rectifier location, coating anomalies, and soil characteristics. The rectifiers, anodic beds, soil compositions, current distribution, etc.

We are building an integrated algorithm not only based on the data field but fundamentals.

Appendix

The experimental test matrix is shown in Table . Base metal and coating were chosen specifically to try and simulate the most commonly used materials in the field. Currently, all lab testing is being performed with 1018 CS base metal and fusion bonded epoxy (FBE) coating that is applied in-house. With plans to include the other base metals and commercially applied coatings. The testing solution for all testing was selected to be NS4 solution with various pH values. This solution simulates the near-soil environment seen in the field and consists of 4 chemicals: sodium bicarbonate ($NaHCO_3$), potassium chloride (KCl), Calcium Chloride ($CaCl_2$), and magnesium sulfate heptahydrate ($MgSO_4$-$7H_2O$). Exact composition and methods for altering pH are detailed below. The cathodic protection (CP) and coating state were varied to simulate the various conditions that in-use pipelines can be found. Understanding how the CP level and coating state affect the impedance response of the system can provide more insight into detecting problems with pipelines earlier and with more accuracy.

Table 1: Experimental Test Matrix

Base Metal	Testing Solution	CP State (mV vs SCE)	Coating	Coating State	Coating Thickness (mil)
1010/1018	NS4 – As-recived	OCP (no protection)	Coal Tar	Intact	15
X52	NS4 – Neutral pH	-637 (under protection)	FBE	Holiday – small	20
X68	NS4 – Acidic pH	-777 (standard protection)	Yellow Jacket	Holiday – large	25
		-1227 (over protection)	Tri-layer	Delamination	35
			4500		25-40

Test Procedure

- <u>Laboratory Testing</u>

1018 carbon steel plates were coated with a commercial-grade FBE. The thickness of the coating was varied from 10 mil to 50 mil. Coating thickness was controlled with a micrometer-adjustable film applicator. Two initial studies were performed with the FBE coatings: 1) effect of coating thickness on impedance response of the system with and without holidays at OCP, and 2) Effect of CP state for a coating with a thickness of 25 mil under the three-coating states (intact, holiday, and delamination). For the initial holiday creation, the holiday was of square geometry and was cut by hand into the coating after the coating was fully cured. The dimensions of the holiday were 0.5 cm x 0.5 cm (0.20" x 0.20"), giving a surface area of 0.25 cm^2 (0.039 in^2). Going forward, all holidays were created with a circular geometry and were cut with an end mill to ensure that the created holidays are consistent. The diameters of the small and large holidays are 0.516 cm (0.203") and 0.794 cm (0.313"), respectively.

The NS4 solution was used as the testing solution to simulate the corrosion of buried pipelines. NS4 is a soil-mimicking solution that consists of potassium chloride (0.122 g/L), sodium bicarbonate (0.483 g/L), calcium chloride (0.137 g/L), and magnesium sulfate heptahydrate (0.131 g/L). To adjust the pH of the solution, various concentrations of CO_2/N_2 were purged through the solution, where increasing the amount of bicarbonate in the solution lowers the pH of the solution [9].

All electrochemical testing was performed at ambient conditions with a three-electrode system. A saturated calomel electrode (SCE) was used as the reference electrode, platinum mesh as the counter electrode, and the tested material as the working electrode. EIS measurements were performed by applying a sinusoidal perturbation while varying frequencies from 100 kHz to 10 mHz. For the intact coating samples, the potential perturbation was set to 15 $mV_{rms,}$ and for samples with defective coatings, it was set to 10 mV_{rms}. A large potential signal was applied to the intact coating samples to increase the current response of the system, lowering the amount of noise in the measurements. To simulate the various levels of CP, the DC bias potential for the EIS signal was set to the specified potentials.

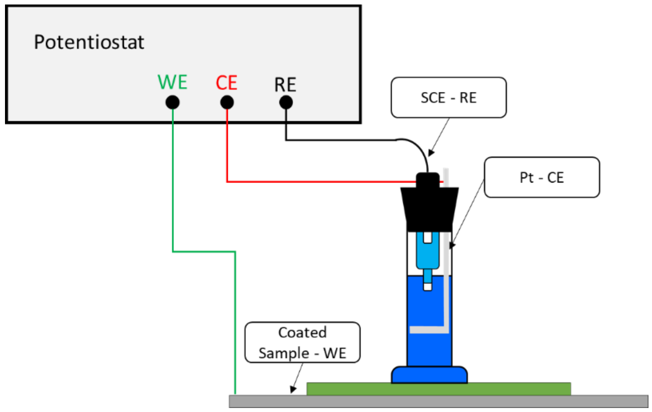

Figure 1: EIS testing schematic

After performing OCP, LPR, and EIS, the samples underwent decay testing. Starting with the OCP measurement, the initial potential was selected in the anodic direction of the process at +0.1V from the OCP. The schematic test system was set up as shown in Figure 1 and 2. The power supply was connected to apply the selected potential condition. The system was held for 30 seconds to ensure stability, after which the power supply was turned off, and the potential was measured using a voltmeter for 600 seconds to confirm that stability remained.

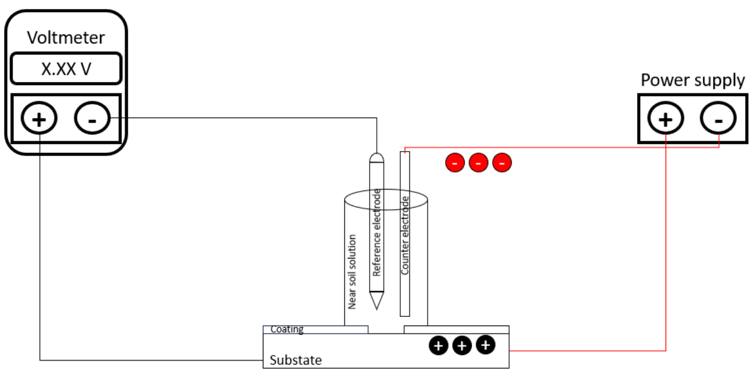

Figure 2: Schematic illustration for the anodic decay setup of the tests

Results and Discussions

Task 1: Designing and building the physical prototypes in laboratory conditions and deterministic modeling

- Task 1.1: Electrochemical Impedance Spectroscopy Study: Lab Data

There is a continued effort to generate data in the lab following the experimental test matrix shown in Table . Figure shows the effect of coating thickness on the impedance response of a coated substrate with two different holiday radii. For all coating thicknesses, there is little deviation in the impedance response between the three coatings for each holiday size. But it can be seen that with the smaller holiday, the overall impedance response is larger compared to the samples with the larger holiday for all coating thicknesses.

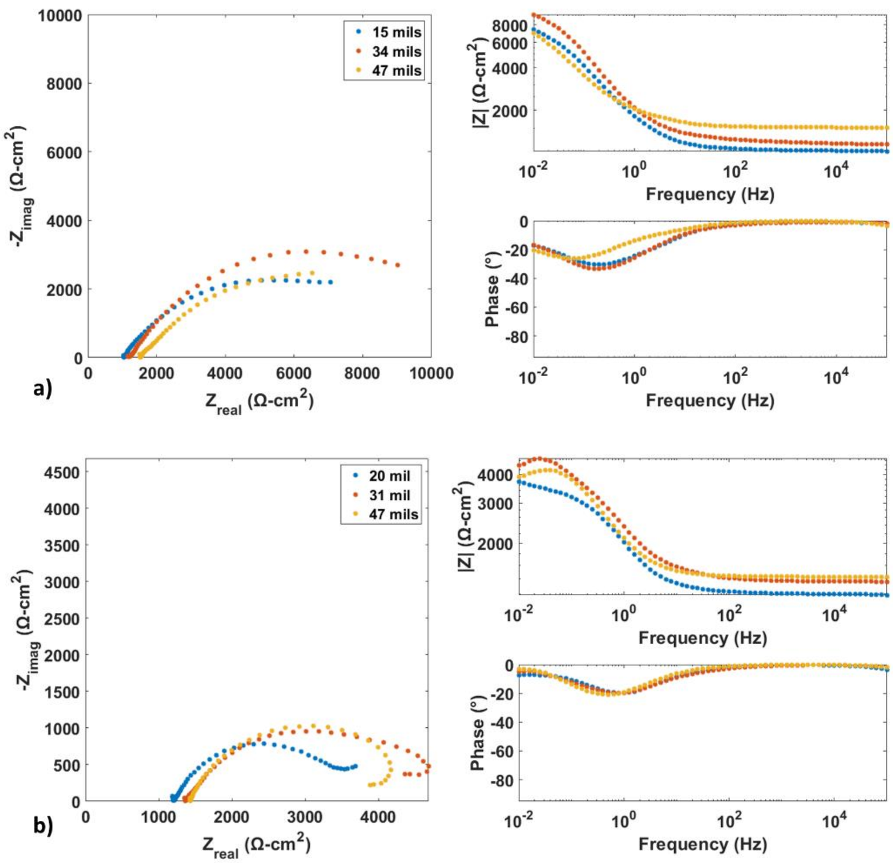

Figure 3 Effect of coating thickness on the impedance response of a coated substrate with a) 0.516 cm and b) 0.794 cm holiday

Figure shows the effect of polarization condition on the impedance response of FBE coatings with and without holidays present in the coating. At all potential values intact coating shows consistently high impedance (10^{10}-10^{12} Ω-cm^2) at low frequencies, with a linear decrease as frequency increases. This indicates excellent barrier properties and capacitive behavior characteristic of an undamaged coating. This is a characteristic response of the highly capacitive coating. The large and small holiday defects display much lower impedance values, by the large drop in overall impedance values and more positive phase angle values. Small holidays consistently show higher impedance values than large holidays across all protection potentials, suggesting better residual protection capabilities. As for the protection potential effect, OCP shows baseline behavior, whereas standard protection provides optimal results for defect mitigation. Both defect sizes show distinctive phase angle peaks in the mid frequency range (10^0-10^2 Hz) when tested at OCP. For under protection, small holiday shows deeper phase angle minima (-40°) and large holiday exhibits shallower phase angle response (-20°). Under standard protection, phase angle minima become more pronounced for both defect sizes. Small holidays show more negative phase angles than large holidays. For overprotection, phase angles become less negative and there is a convergence of phase response between large and small holidays. This reduction in phase angle variation shows more resistive behavior

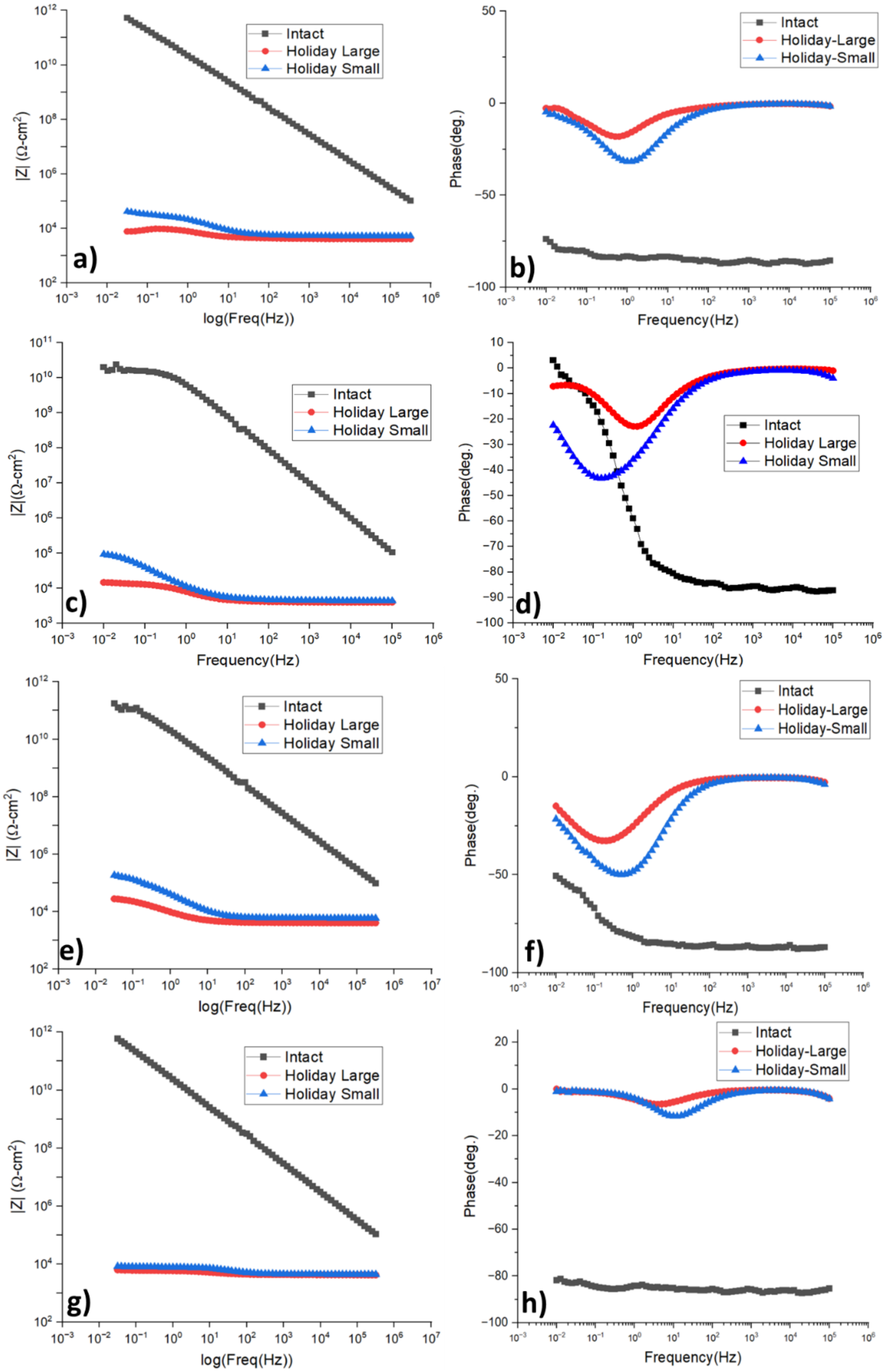

Figure 4: Bode and phase angle plots for FBE coatings with and without holidays for various CP conditions (a-b) open circuit conditions, (c-d) under protection, (e-f) standard protection, and (g-h) over protection

Figure shows the effect of polarization condition on the impedance response of coal tar coatings with and without holidays present in the coating. The intact coating showed consistently high impedance (10^{10}-10^{12} Ω-cm^2) at low frequencies similar to FBE. These high values were shown for each polarization condition as well. The phase angle behavior for intact coating exhibits near-capacitive behavior approaching 90° and shows minimal frequency dependence in mid to high frequency ranges. Defect responses in coal tar show clearer separation between the intact and damaged coating conditions. Applying the under protection potential for the coal tar coating defects did not produce a drastic change from the OCP conditions. But, applying standard protection did increase the overall impedance relative to the under protection potential and OCP conditions. For the over protection potential the overall impedance did drop but is most likely due to the higher rate of cathodic reaction occurring with the larger more negative potential that was applied to the surface.

The overall impedance response was very similar for the two coatings when various cathodic protection potentials were applied. The intact coatings showed large impedance values and phase angle values near -90° for most of the frequency domain regardless of the potential application. There was little difference between the impedance response between OCP and under protection potential for FBE and coal tar coatings. This is most likely due to OCP and under protection potential being similar in magnitude. Impedance measurements under the standard protection potential did show an increase in the impedance magnitude and more negative phase angle values for both small and large holidays. This is indicative that the exposed surface was more protected with the application of the standard protection potential. For both FBE and coal tar coatings when the overprotection potential was applied the impedance magnitude decreased and phase angle values became more positive. This is most likely due to the increased cathodic reaction rate with a more negative potential relative to the other three conditions.

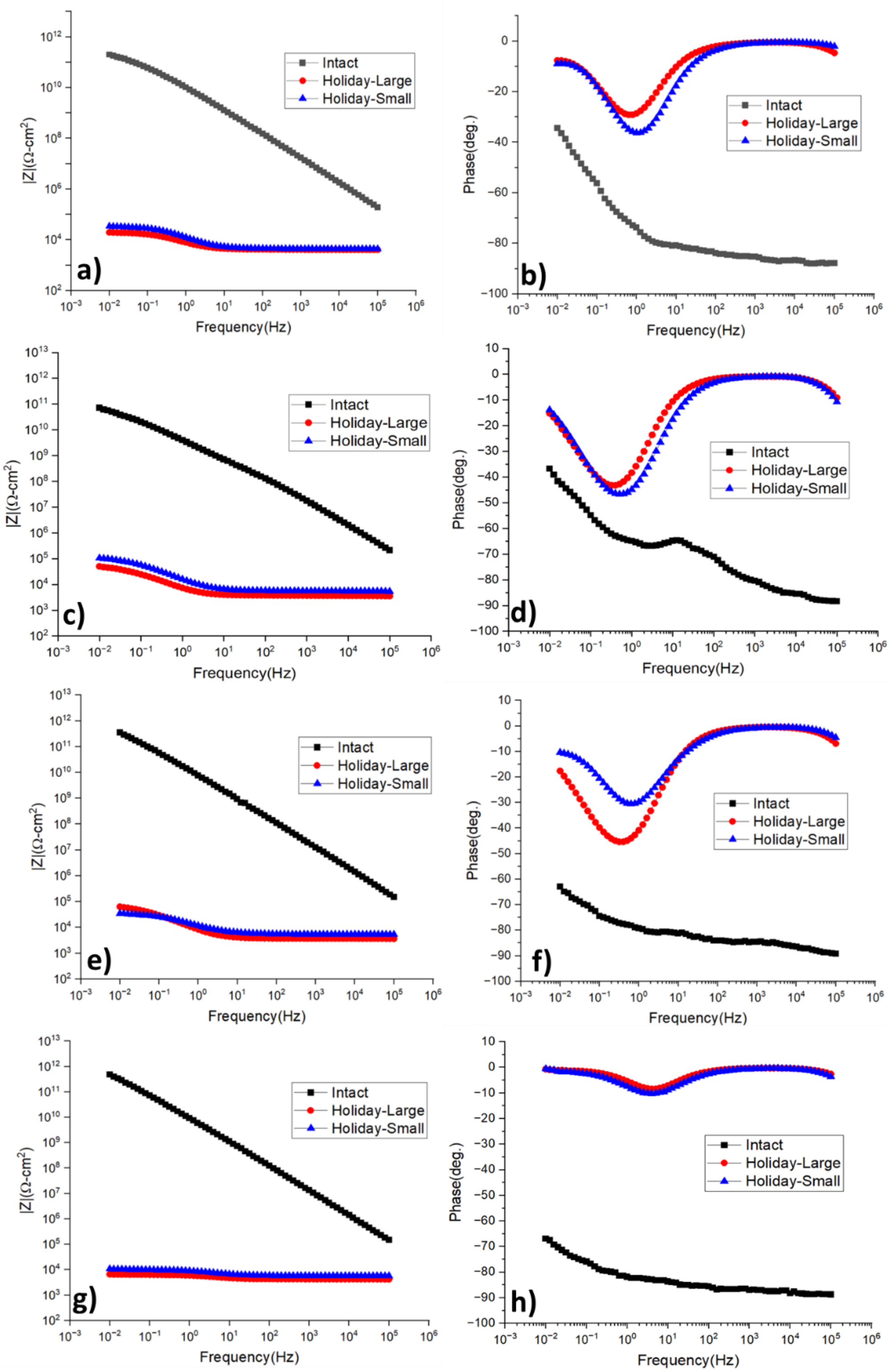

Figure 5: Bode and phase angle plots for Coal Tar coatings with and without holidays for various CP conditions (a-b) open circuit conditions, (c-d) under protection, (e-f) standard protection, and (g-h) over protection

Figure 6 presents the Bode and phase angle plots for 4500 coating with a thickness of 25 mils under various CP conditions. The intact coating maintains high impedance values at low frequencies, like other coatings, indicating strong barrier properties. Defect responses show a notable decrease in impedance compared to intact coatings, with small holidays generally exhibiting higher impedance than large ones. Under standard protection, impedance increases, and phase angles become more negative, suggesting enhanced protection of the exposed surface. Overprotection leads to decreased impedance and less negative phase angles, indicating increased cathodic activity. The plots suggest that standard protection is most effective for mitigating defects in these coatings.

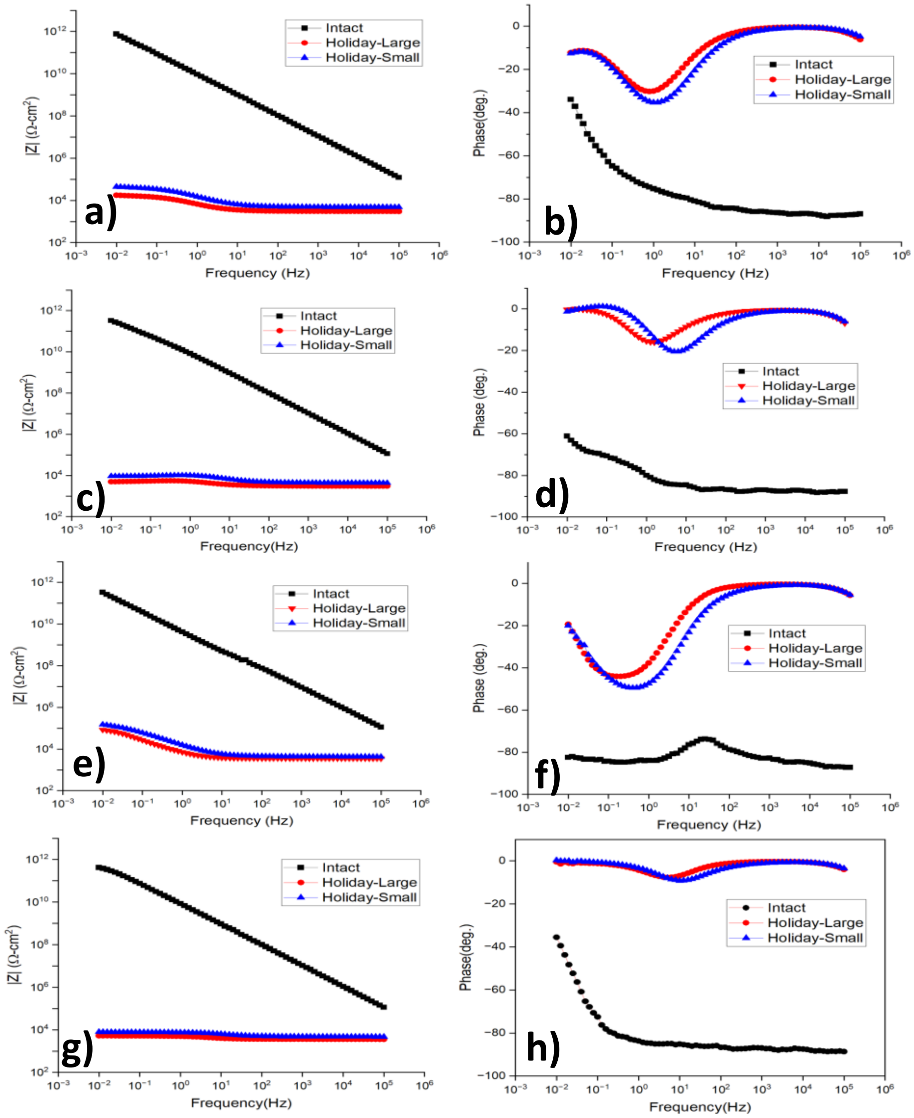

Figure 6: Bode and phase angle plots for 4500 coating (25 mils thickness) coatings with and without holidays for various CP conditions (a-b) open circuit conditions, (c-d) under protection, (e-f) standard protection, and (g-h) over protection

Figure 7 shows similar trends for a 4500 coating with a thickness of 40 mils. The thicker coating maintains high impedance at low frequencies, consistent with other coatings. Defect responses are more pronounced, with small holidays showing higher impedance than large ones across all protection conditions. Standard protection enhances impedance and phase angle responses, indicating better defect mitigation. Overprotection results in decreased impedance and less negative phase angles, likely due to increased cathodic reactions. The thicker coating may offer slightly better barrier properties, but the overall trends are consistent with thinner coatings.

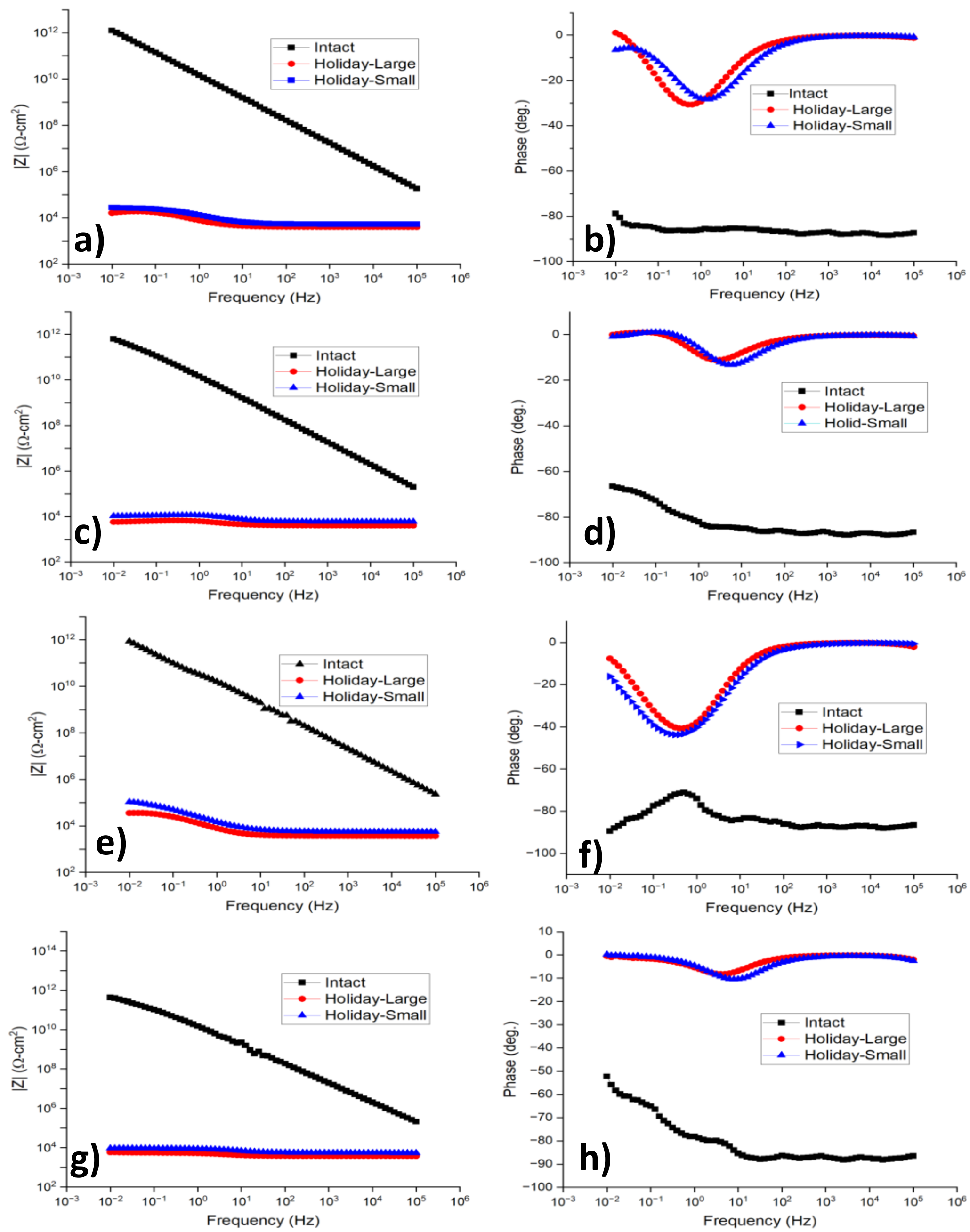

Figure 7: Bode and phase angle plots for 4500 coating (40 mils thickness) coatings with and without holidays for various CP conditions (a-b) open circuit conditions, (c-d) under protection, (e-f) standard protection, and (g-h) over protection

All three coatings exhibit high impedance values at low frequencies when intact, indicating strong barrier properties. Standard protection generally enhances impedance and phase angle responses, suggesting better defect mitigation. Overprotection leads to decreased impedance and less negative phase angles due to increased cathodic reactions. The coal tar coatings show clearer separation between intact and damaged conditions compared to FBE coatings. The 4500 coating, regardless of thickness, follows similar trends to the other coatings but may offer slightly better barrier properties due to its thickness. Overall, standard protection is most effective for mitigating defects in these coatings.

- <u>Task 1.2: Fitting 2D TLM to the Lab data – EEC Fitting</u>

This is an initial set of data that was performed with the square holiday geometry as a proof of concept. Figure shows the Nyquist, Bode, and phase angle plots of FBE-coated carbon steel after 1 week of immersion and the fitted 2D TLM. The coated samples displayed phase angle values near -90°, which shows that the coating behaves like a perfect capacitor and still protects the base material. The EEC values determined from CNLLS fitting are shown in Table . The fitted values of the EEC were able to fit the experimental data relatively well, showing the viability of the model for use with high impedance systems. In the low frequency regime, it can be seen that the phase angle starts to bend towards more positive values. This shift in phase angle values is most likely due to water uptake into the coating. This displays the ability of the model to still perform well when the impedance of the electrodes tends towards non-ideal behavior.

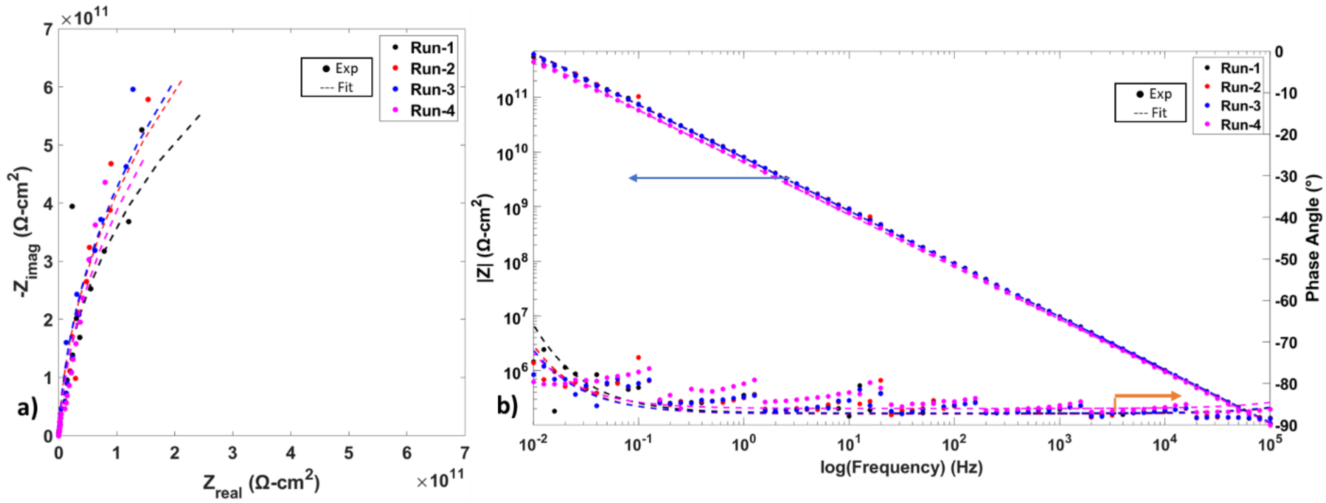

Figure 8: a) Nyquist and b) Bode and phase angle plots of coated carbon steel in NS4 solution after 1 week immersion

Table 2: CNLLS Fitted values of EEC values used in 2D TLM for coated carbon steel in NS4 solution

Sample	*R (Ω-cm²)*	*Q (F-cm²-s⁻ⁿ)*	*n*	*RMS Error*
Run 1	$1.69 * 10^{12} \pm 1.37 * 10^{11}$	$2.17 * 10^{-11} \pm 2.74 * 10^{-13}$	0.968 ± 0.0015	0.0716
Run 2	$2.29 * 10^{12} \pm 2.92 * 10^{11}$	$2.14 * 10^{-11} \pm 2.55 * 10^{-13}$	0.970 ± 0.0014	0.0682
Run 3	$2.44 * 10^{12} \pm 2.95 * 10^{11}$	$2.17 * 10^{-11} \pm 2.17 * 10^{-13}$	0.969 ± 0.0012	0.0575
Run 4	$2.19 * 10^{12} \pm 3.84 * 10^{11}$	$2.68 * 10^{-11} \pm 3.41 * 10^{-13}$	0.956 ± 0.0015	0.0735

The EIS measurements of coated samples with a holiday introduced after one week of immersion is shown in Figure . It can be seen that there is a drastic decrease in the overall impedance of the system compared to the impedance of the intact coating shown in Figure . In the model, $\mathbb{R}_1$ was defined as the intact coating, an average value of the fitted EEC values from case 2 was used as the EEC values in $\mathbb{R}_1$. For the $\mathbb{R}_2$ the values were changed to provide the best fit possible. Initially, the CNLLS function is not able to provide fitting for the heterogeneous case, so fitting was performed manually; fitted EEC values are shown in Table . The model was able to provide the best fit in the medium to low frequency ranges ($< 10^1$ Hz) and still had trouble with fitting in the high frequency regime, most likely due to the system not considering systemic/random errors that can occur during measurements.

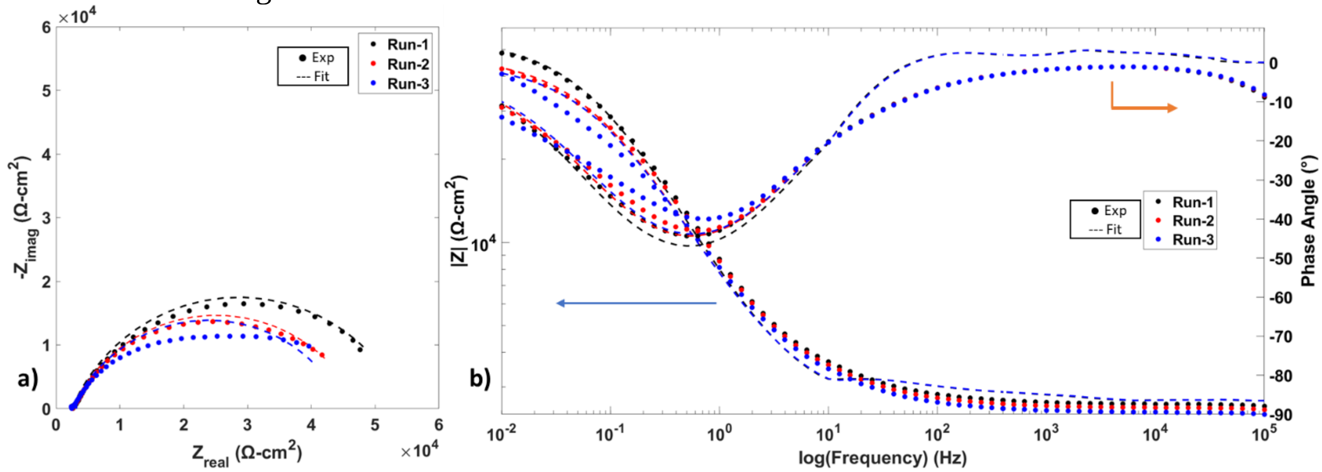

Figure 9: a) Nyquist and b) Bode and phase angle plots of coated carbon steel with coating holiday in NS4 solution after 1 week immersion

Table 3: Fitted values of EEC values used in 2D TLM for coated carbon steel with coating holiday in NS4 solution

Sample	*Region*	*R* *(Ω-cm^2)*	*Q* *(F-cm^2-s^{-n})*	*n*	*RMS Error*
Coating	$\mathbb{R}_1$	$6.86 * 10^{11}$	$7.19 * 10^{-11}$	0.966	-----
Run 1	$\mathbb{R}_2$	$1.73 * 10^{4}$	$1.10 * 10^{-3}$	0.750	0.1012
Run 2	$\mathbb{R}_2$	$1.49 * 10^{4}$	$1.18 * 10^{-3}$	0.733	0.1104
Run 3	$\mathbb{R}_2$	$1.41 * 10^{4}$	$1.18 * 10^{-3}$	0.733	0.1367

Traditionally a lumped EEC would be used for fitting the EIS data even when there are known heterogeneities in the system. Using the same EEC structure as was used in the 2D TLM, a lumped EEC was fit to the experimental data for comparison. The EEC values obtained by traditional lumped EEC circuit fitting is shown in Table .

Table 4: Lumped EEC fitting values

Sample	*R* *(Ω-cm^2)*	*Q* *(F-cm^2-s^{-n})*	*n*
Run 1	$3.84 * 10^{4}$	$3.58 * 10^{-4}$	0.700

Run 2	$4.56 * 10^4$	$3.70 * 10^{-4}$	0.691
Run 3	$4.33 * 10^4$	$4.28 * 10^{-4}$	0.654

Both the resistance and Q values of the lumped EEC values are somewhere between the values used for the two regions shown in Table . This is most likely due to the lumped EEC taking an average of all the processes occurring with accounting for both the holiday and intact coating separately. The fitted resistance value is around two times higher in the lumped EEC compared to 2D TLM. This could lead to an underestimation of the extent of corrosion that is occurring at the holiday when calculating the local corrosion rate of the metal.

The |Z| and phase angle distributions at 10 Hz for the coating with the square holiday is shown in Figure . The black lines indicate the model geometry. Outside the square is assumed to be the intact coating ($\mathbb{R}_1$) and inside the square is assumed to be the holiday ($\mathbb{R}_2$). Both the |Z| and phase angle distributions display steady changes from the boundary of the model to just outside of $\mathbb{R}_2$, and then stays relatively constant inside of $\mathbb{R}_2$, and remained relatively constant inside of $\mathbb{R}_2$.

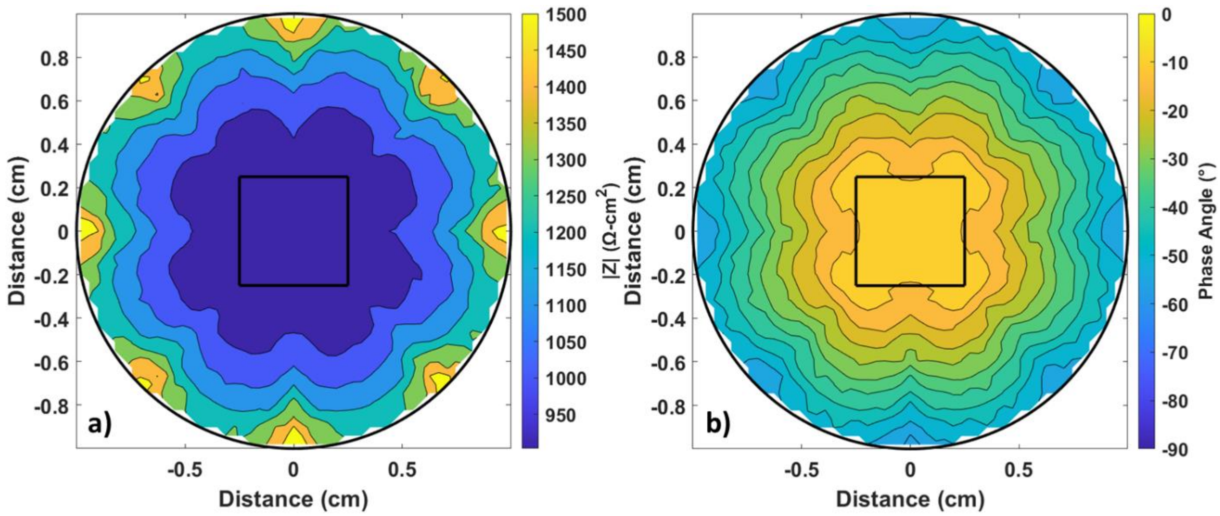

Figure 10: a) |Z| and b) phase angle distribution from 2D TLM at 10 Hz for coating with a holiday. Where the 2D TLM EEC values for the two regions are: $\mathbb{R}_1$ EEC values: $\boldsymbol{R = 2.18 * 10^{11}\ \Omega}$, $\boldsymbol{Q = 2.26 * 10^{-10}\ F - s^{-n}}$, $\boldsymbol{n = 0.966}$ and $\mathbb{R}_2$ EEC values: $\boldsymbol{R = 1.57 * 10^3\ \Omega}$, $\boldsymbol{Q = 1.17 * 10^{-4}\ F - s^{-n}}$, $\boldsymbol{n = 0.739}$

- <u>Task 1.3: Fitting 2D TLM to the Lab data – Mechanistic Model</u>

Figure , Figure displays the 2D TLM ability for using mechanistic definitions to fit data from an intact coating with various thickness and a 15 mil coating with a defect in the center of the exposed area. From Figure it can be seen that the impedance response of the 2D TLM using mechanistic definitions for the coating capacitance was very similar to that of the experimental data. The difference between the model and experimental data is due to the model assuming a homogenous value of the coating thickness and ohmic resistance of the coating. Unlike the actual case there is a distribution of these across the interface which creates a deflection of the data from its ideal behavior. Overall the model was able to produce a similar impedance response that was seen in the intact coating case. The biggest defect occurred in the thicker coating. This is most likely due to the thicker coating that was applied to the substrate; with a thicker coating, there is a more likely chance that the coating has some sort of defect that can influence the impedance response of the system. Also, with this first case of fitting the ohmic resistance of the coating was not changed from sample to sample in the 2D model, but most likely there is some deviation of ohmic resistance between the actual coated samples that needs to be taken into account for a better fit. As of right now, there is no model that is applied for determining the ohmic resistance of the coating; the value is just an assumed value in the 2D model.

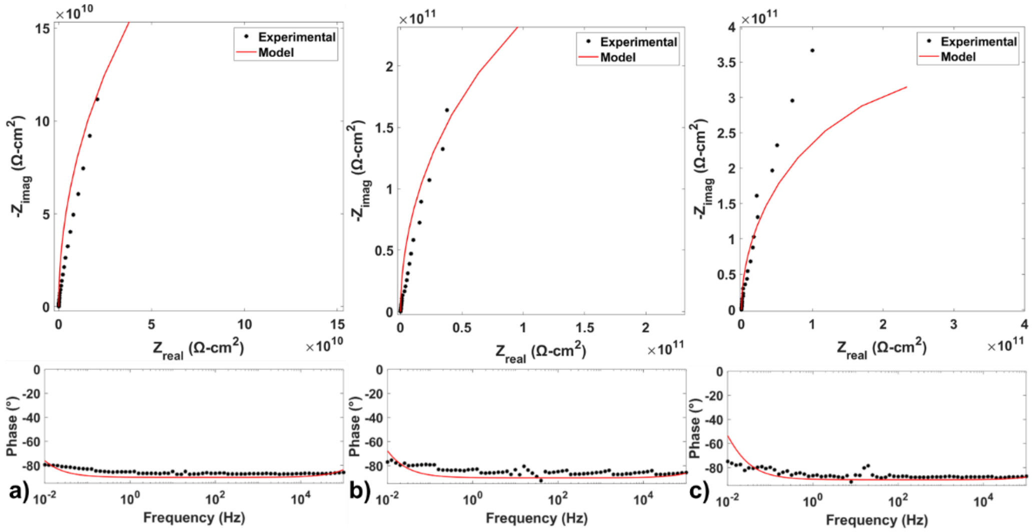

Figure 11: Nyquist and phase angle plots comparing experimental and model results for a) 15 mil, b) 25 mil, and c) 45 mil coatings.

Figure shows the comparison of the 2D model with experimental results for a 15 mil FBE coating that had a holiday introduced into the coating exposing the substrate. Two initial measurements were performed on two separate locations and this data was used to check the validity of the model's output. From Figure it can be seen that the 2D model was able to give a pretty good estimation of the general form of the impedance response of the system. The deviation between the model and experimental data is most likely due to the model assuming a idealized impedance response and assuming one time constant for the entire surface. In actuality there is a distribution of time constants in the experimental results that creates the deflection from idealized impedance response. To create a better fit of the model to experimental data it must be assumed in the model that there is some distribution of time constants.

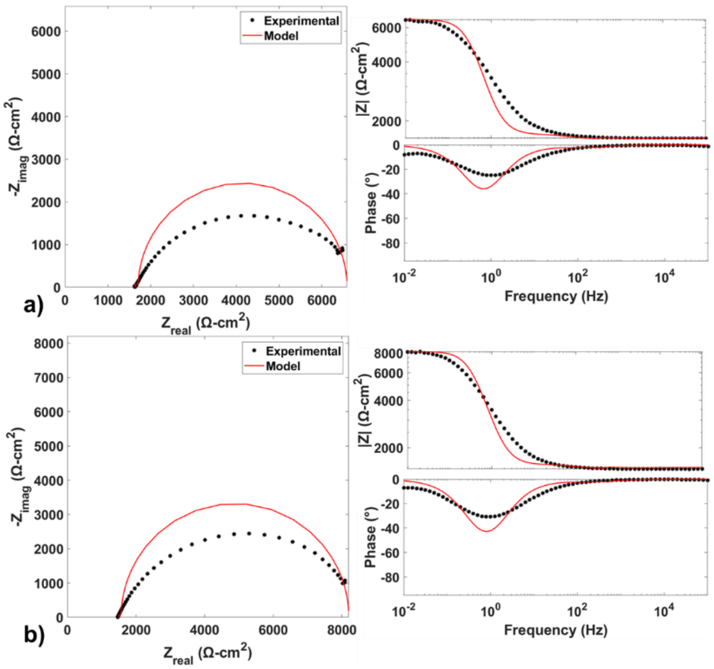

Figure 12: Nyquist, Bode, and Phase angle plots of two different 15 mil FBE coatings with a defect with an area of 0.275 cm^2

References

1. Huang, V.M.-W., et al., *The apparent constant-phase-element behavior of an ideally polarized blocking electrode: a global and local impedance analysis.* Journal of the Electrochemical Society, 2006. **154**(2): p. C81.
2. Brug, G., et al., *The analysis of electrode impedances complicated by the presence of a constant phase element.* Journal of electroanalytical chemistry and interfacial electrochemistry, 1984. **176**(1-2): p. 275-295.
3. Tsai, Y.-T. and D. Whitmore, *Nonlinear least-squares analyses of complex impedance and admittance data for solid electrolytes.* Solid state ionics, 1982. **7**(2): p. 129-139.
4. Marquardt, D.W., *An algorithm for least-squares estimation of nonlinear parameters.* Journal of the society for Industrial and Applied Mathematics, 1963. **11**(2): p. 431-441.
5. Alper, J.S. and R.I. Gelb, *Standard errors and confidence intervals in nonlinear regression: comparison of Monte Carlo and parametric statistics.* Journal of Physical Chemistry, 1990. **94**(11): p. 4747-4751.
6. Boukamp, B.A., *A nonlinear least squares fit procedure for analysis of immittance data of electrochemical systems.* Solid state ionics, 1986. **20**(1): p. 31-44.
7. Macdonald, J.R. and J. Garber, *Analysis of impedance and admittance data for solids and liquids.* Journal of the Electrochemical Society, 1977. **124**(7): p. 1022.
8. Sheppard, R., B. Jordan, and E. Grant, *Least squares analysis of complex data with applications to permittivity measurements.* Journal of Physics D: Applied Physics, 1970. **3**(11): p. 1759.
9. Gadala, I.M. and A. Alfantazi, *Electrochemical behavior of API-X100 pipeline steel in NS4, near-neutral, and mildly alkaline pH simulated soil solutions.* Corrosion Science, 2014. **82**: p. 45-57.